Contents lists available at GrowingScience

Engineering Solid Mechanics

homepage: www.GrowingScience.com/esm

Performance of aggregate sizes on crack bridging and capacity enhancement of deep beams

Ajibola Ibrahim Quadri[a*], Razor Robert Bassey[b], Williams Kehinde Kupolati[a], Chris Ackerman[a], Jacque Snyman[a] and Julius Musyoka Ndambuki[a]

[a]*Department of Civil Engineering, Tshwane University of Technology, Pretoria 0183, South Africa*
[b]*Department of Civil and Environmental Engineering, The Federal University of Technology, Akure. Nigeria. P.M.B 704, Ondo State*

ARTICLEINFO

Article history:
Received 8 June 2024
Accepted 18 December 2024
Available online
18 December 2024

Keywords:
Aggregate interlock
Aggregate sizes
Damage mode
Deep beams
Finite element model
Reinforced concrete
Shear estimation
Shear performance

ABSTRACT

Reinforced concrete deep beams (RCDBs) investigations are often complex because of the highly disturbed zones which may aggravate the shear performance under variable loadings. The shear capacity enhancement of RCDB using different aggregate sizes of 19 mm, 25 mm, and 50 mm has been investigated under three-point monotonic loading. Nine RCDBs with 750 × 170 × 225 mm dimensions were considered, and the beam was loaded at a 1.4 shear span to depth ratio. Three of the beams were designed without web reinforcement, and six were designed for web reinforcement with varied aggregate sizes. There was no significant difference in the shear strength of RCDBs considered however, a 50 mm aggregate beam was found capable of reducing the multiple crack propagations when compared to other aggregate-size beams. Additionally, the shear reinforcement increased the ductility and strength by over 30% and 20%, respectively. The applicability of 3-dimensional FEM extended to the investigation acceded with the shear response of the experiment exercising shear stiffening behavior. The estimated model from the modified ACI 318:05 can predict the shear capacity of the RCDB with higher accuracy. Since aggregate resists the load by aggregate interlock action, it is crucial to choose the right aggregate when building concrete structural components. The results of this study will help engineers choose the best aggregate for a certain structural element.

1. Introduction

Infrastructural development is an integral component of the economic growth of any nation worldwide. Hence, no construction activities can be imagined without concrete in the present day (Quadri et al., 2023). It is arguably the most utilized material in the construction industry because of the cheap constituent materials. However, over 10 billion tons of concrete are produced worldwide annually (Hasan et al., 2023). It is also the second most adopted material in the world after water (Meyer, 2009). Concrete is a man-made heterogeneous material that constitutes water, aggregates, cement, and pore structures in different proportions based on strength requirements. The tensile strength of concrete accounts for approximately 10% of its compressive strength, resulting in poor performance under tension load (Quadri, 2023a). While cement binds the other materials in the concrete matrix by a coating process, coarse aggregate occupies over 50% volume of the concrete matrix offering great strength in resisting external forces and is usually retained in a 4.75 mm sieve (sieve No. 4) (Nehdi, 2014). The coarse aggregate properties rarely limit the strength of a typical concrete mixture with a water-cement ratio (w/c) between 0.5 and 0.7. The transition zone between cement paste and coarse aggregate is the weakest zone; however, in high-strength concrete, the hardened cement paste and transition zone do not form the strength limit; instead, it is the mineral constituents and coarse aggregate strength that control the strength of concrete (Beshr et al., 2003). Thus, the quality of coarse aggregate in concrete is essential when considering the quality of concrete for durability and structural performance.

Different sizes of aggregates are produced in quarries for construction work; however, the suitability of these aggregates is rarely tested to determine their integrity and performance in structural elements. As the population and economic activities

* Corresponding author.
E-mail addresses: quadriai@tut.ac.za (A. I. Quadri)

ISSN 2291-8752 (Online) - ISSN 2291-8744 (Print)

doi: 10.5267/j.esm.2025.1.001

grow, so does the need for housing. Building collapse is on the rise as the usage of materials, mainly concrete for structures, increases partly due to low-quality construction materials, defective design, and construction due to excessive accretion of money from material production or construction process.

Different researchers have tested the performance of coarse aggregate in concrete production. Apebo et al. (2013) identified river-washed gravel as the most commonly used coarse aggregate due to the presence of river deposits. The washed gravel was mixed with burnt bricks at a (w/c) of 0.5. The 28-day compressive strength of 21 N/mm^2 was achieved. Lowering the w/c to 0.48, Bhattacharjee et al. (2011) achieved a compressive strength of 29.2 N/mm^2. Although washed gravel may not be available in areas not served by the river, the expense of transporting alternative materials outside the catchment area may raise the cost of building even when labor is cheap. Bamigboye et al. (2016) evaluated the appropriateness of using locally available material instead of crushed granite aggregate for concrete sustainability. 10 mm and 20 mm aggregates were used and classed as washed and unwashed. The results showed that the washed smaller aggregate has the highest compressive strength value of 29.7 MPa, whereas the unwashed 20 mm aggregate has the lowest value of 24.5 MPa after 28 days of curing age. Thus, aggregate grading, sizes, and internal bonding all contribute to the strength of concrete.

The present research adopts three different sizes of aggregates (19 mm, 25 mm, and 50 mm) to understand the performance of aggregate sizes in crack bridging and shear capacity enhancement of RCDBs under increasing monotonic loading. Deep beams are beams with large depths to the spans. A study by Abtan and Hassan (2020) defined deep beams as having depths much greater than seen in regular beams to their span. RCDB has been defined to have an overall span-to-depth ratio (l/d) less or equal to 4, or the effective shear span-to-effective depth ratio (a/d) equal or less than 2 and 2.5 for a continuous beam (Reddy et al., 2019). The effective span is defined as the center-to-center (c/c) distance between the supports (Kore & Patil, 2013). RCDBs are qualified to possess (a/d) relatively small thus, their response to applied load is dominant in shear than in flexure, and their capacity relies on the mode of applying load and support conditions (Quadri, 2020; Alius et al., 2020). Several codes of practice are used for the design purposes of structures; however, some provide little information about the behavior of deep beams. By definition, BS 8110-97 (BS 8110, 1997) part 1 refers to a deep beam as any beam having a clear span less than twice its effective depth. Eurocode 2 (EN-2) (*Eurocode 2*, 2008) defines a deep beam as any beam whose overall span is less than three times its overall section depth. EN-2 does not directly provide guidelines for the design of deep beams; it refers instead to clause 18.1.8 of the CEB-FIP model 1978 (Institute of Civil Engineers, 1993). The CEB-FIB model code applies to simply supported beams of span/depth ratio l/d less than 2 and continuous beams of l/d less than 2.5. Some scholars such as Daneshfar et al. (2022,2023a,b) and Hoseini et al. (2022,2023a,b, 2024) and Mousavi et al. (2024), Xu et al. 2(021), Accornero et al., (2022), Golewski, (2023); Gand et al. (2019,2020) have investigated the flexural toughness, cracking mechanism, failure initiation and post peak failure mechanisms of concrete beams and discs made of different fibres and additives subjected to bend loading

RCDBs have proven to be very useful in construction works as their areas of application in building structures range from transfer girders to foundation pile caps, wall footings, and shear walls. Deep beams are also used as perimeter beams for reinforced concrete frames for structural and architectural function (Kim et al., 2009). Chen et al. (2019) described deep beams as one of the main loads carrying structural members and are used in the construction of high-rise buildings, bridge structures, and underground structures. However, RC deep beams experience shear cracking which can result in total failure when subjected to loading because of the presence of a high disturbed region. Brittle failure results from the rapid development and steep propagation of shear cracks (Yang et al., 2025). Due to the low shear span-to-depth ratio, the conventional flexural design principles are not applicable (Megahed, 2024; Liu & Mihaylov, 2020). Furthermore, the distribution of stresses across the weakest zone of deep beams is nonlinear, deviating from the typical linear distribution assumed in shallow beam design which implicates the analysis and can lead to inaccurate prediction of shear strength.

The specific effects of various coarse aggregate types and their physical characteristics on the shear capacity of reinforced deep beams are still unknown despite a great deal of study on aggregate concrete (Cho & Kim, 2024). Concrete compressive strength, depth-to-width ratio, and web reinforcement ratio can all significantly impact the shear strength of deep beams, with an increase in the shear span-to-depth ratio (Ma et al., 2022) al. Yang et al. (2003) studied the shear properties of twenty-one high-strength RCDBs with the factors of concrete strength, a/d, and overall depth, based on the strength at the first diagonal fracture of normal strength beams recommended by ACI code (ACI Committee 318, 1999) on size effect. The drop in a/h and rise in total depth caused brittle failure, characterized by wide cracks and substantial energy release in size effect concerns. It was discovered that sensitivity to size affected is lower at a/h = 0.5 than at a/h = 1. The increase in concrete strength seen in the study was not proportional to the rise in shear strength of deep beams, demonstrating that high-strength RCDBs can display size effects with brittle failure. Farouk et al. (2023) examined six sets of RCDBs with web holes, three of which were internally strengthened with steel plates and the others externally reinforced with fasteners. The parameters tested were load capacity, deflection, crack patterns, and stiffness. The size, position, and geometry of the apertures influence the performance of the beams, resulting in a reduction in stiffness and load capacity. Externally strengthening the web aperture can help boost beam capacity. Saleh et al. (2023) also stated that the cross-section, size, and position of the web opening of deep beams have a significant impact on their behavior; nonetheless, reducing the shear span to depth ratio and increasing concrete compressive strength can improve the ultimate load. Alqarni et al. (2022), used various coarse aggregates manufactured from 10 mm limestone, quartzite, and 20 mm steel slag heavy-weight aggregate for deep beam casting. Temperatures of 25^{o}C and 600^{o}C

were used to test the specimens. Eight of the specimens were designed to fail in shear, four to fail at room temperature, and four to fail at an elevated temperature of 600ºC for three hours. The results showed shear damage similar to aggregate abrasion, while high-temperature exposure reduced shear capability based on the coarse aggregate type. Limestone aggregate can withstand higher temperatures than steel slag and quartzite, with shear reductions of 23%, 37%, and 45%, respectively.

Several researchers have also predicted the shear performance of RC deep beams (Abadel et al., 2022; Campione and Minafò, 2012; Chen et al., 2018; El-Demerdash et al., 2016; Ibrahim et al., 2018; Mohamed et al., 2014; Quadri, 2023b). Chen et al. (2018) investigated the shear behavior of deep beams under static loading to failure. Ten steel reinforced concrete (SRC) beams of I-section steel together with two normally reinforced concrete deep beams were considered. The steel section was fabricated following ASTM A36 hot-rolled steel shapes and shape plates. It was reported that the flange may contribute significantly to the shear capacity and ductility of the deep beams. Although no composite action exists in the SRC deep beam, the SRC exhibited higher shear strength than the non-composite SRC deep beam by up to 23%. In research by Albidah et al. (2023a), the influence of coarse aggregate behavior on the performance of nine RC deep beams has been examined. Three coarse aggregate types, limestone, steel slag, and quartzite having sizes of 10 mm and 20 mm were used. The beams were loaded statically under four-point loading. The bigger aggregate reduced the number of cracks propagation in the beams however, the aggregate does not influence the stiffness and the rigidity of the beam. The influence of aggregate characteristics on deep beam performance has been investigated (Alqarni et al., 2022), which revealed that the stiffness of deep beams is not affected by different aggregate but improved the shear strength.

One of the ways the capacity of a structure can increase is through aggregate interlock, the use of different aggregate sizes to enhance the shear capacity of deep beams is not common in literature, it is, therefore, important to understand the effect of different aggregate sizes on the performance of deep beams under increasing monotonic loading. In addition, empirical assessment and computational modeling of reinforced concrete structures are commonly employed to investigate concrete structures' nonlinear behavior. Although the empirical approach yields accurate results, it can only explain phenomena in specific geometries, applied load, and cost. (Quadri, 2023a; Quadri and Fujiyama, 2021). The modeling can aid in the extension of the stated features with a viable economy. The study extends the applicability of using a finite element model (FEM) to explore the behavior of deep beams of various aggregate sizes to understand the softening features of RC deep beams. The experiment employs aggregate sizes of 19 mm, 25 mm, and 50 mm, these are the commonly used aggregates for construction of concrete structural members as specified by ASTM (ASTM C33/C33M-18, 2024). Furthermore, a predictive model using a modified shear equation of ACI 318:05 (ACI 318:05, 2005) has been developed for the shear capacity of deep beams with and without web reinforcement.

2. Methodology

2.1 Specimen detailing and casting

A total of nine RCDBs with dimensions 170 × 225 × 750 mm width, depth, and length, respectively loaded at a/d =1.4 were tested for this investigation. Three singly reinforced beams (without web reinforcement) with 10 mm diameter (Ø) reinforcing bars having different aggregate sizes (19 mm, 25 mm, and 50 mm) were cast, the remaining six beams have web reinforcement of Ø8 mm at a spacing of 100 mm c/c. The tensile and the yield strength of the reinforcement of Ø8 mm are 521 and 386 N/mm^2 while that of Ø10 mm are 540 and 416 N/mm^2, respectively. The process goes with the recommendation of BS 8110 (*Structural Use of Concrete*, 1997) design. The 28 days of compressive and splitting tensile strengths of concrete were determined for all the aggregates using cube mold size of 150 mm^3 and 200 × 100 mm height and diameter cylindrical mold cast together with beams using water-to-cement ratio of 0.5 and concrete mix ratio of 1:2:4 following BS EN 12390-5 (BS EN 12390-5, 2009). The beams were cast on the same day, the fresh concrete was placed and compacted inside the dedicated mold, which was allowed to set before demolding after 24 hours. The specimens were then transferred into the curing room under 20ºC, wrapped in curing bags, and wet with water regularly for 28 days. This process of curing was adopted due to challenges of continuous water application. The curing bag maintains moisture directly around the concrete surface and prevents rapid evaporation and reduces water consumption (Quadri, 2021). The curing bag was removed thereafter to eliminate excess moisture for 24 hours at room temperature before being transferred for testing. The strength properties including the compressive and tensile strength values are listed in **Table 1**.

An aggregate crushing value (ACV) test was performed following the recommendation of BS 812-121 standard (BS 812-121, 1975). 3 kg of coarse aggregate passing through a sieve 12.5 mm and retained on 10 mm was acquired and heated up to 4 hours at about 110ºC and cooled at room temperature. The cooled aggregate is placed inside a 25 cm cylinder with plunger and a base plate filled in 3 layers and compacted. The weight of the cylinder before and after the sample was placed was measured and recorded. The compressed sample was then sieved using 2.36 mm and measured. The ACV of 19 mm, 25 mm, and 50 mm aggregates are listed in **Table 1**, The typical ACV recommended by the standard for the surface course should not exceed 30%. The result revealed that the aggregates used are excellent and can absorb considerable load.

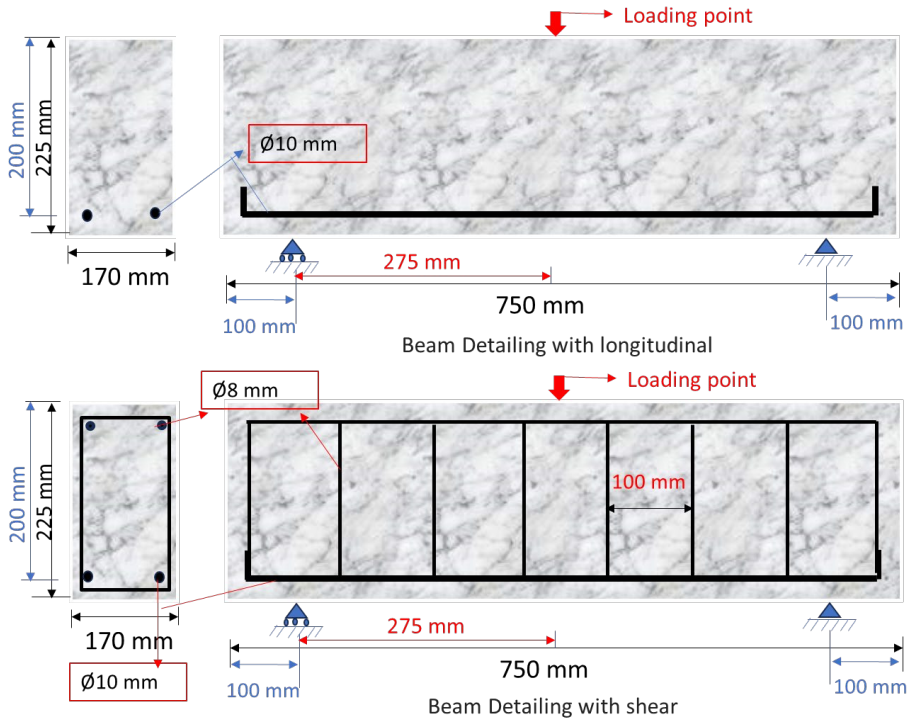

Fig. 1. Reinforcing bars detailing of beam specimens

Table 1. 28 days concrete strength values

S/N	Aggregate size (mm)	Compressive strength (N/mm^2)	Splitting tensile Strength (N/mm^2)	ACV %
1	19	15.6	2.1	23.7
2	25	24	2.4	27.4
3	50	18.7	2.3	25.2

2.2 Specimen loading

Three-point bending tests were performed on the RCDBs with increasing monotonic loading at 10 kN/min on a universal testing machine (UTM) of 300 kN capacity. The crack initiation and propagation zones were observed by visual examination, while the crack width was measured after the final damage. The vertical deflection of the beam was monitored by linear variable displacement transducers (LVDTs) placed in the middle (underside of the loading point) as shown in **Fig. 2**.

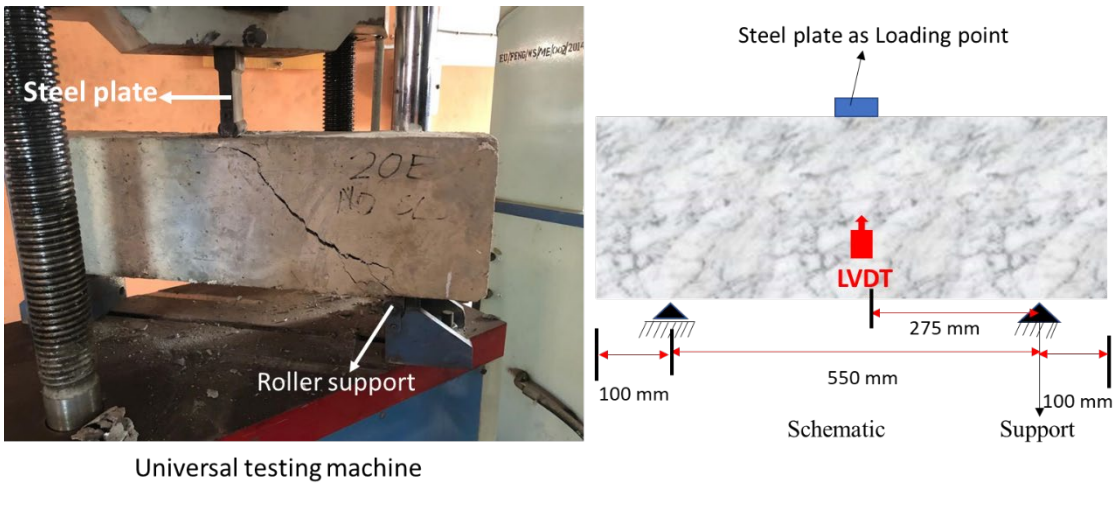

Fig. 2. Experimental loading setup for RCDB

2.3 Finite element discretization of deep beams with different aggregate sizes

A three-dimensional nonlinear finite element approach was utilized in this study for the modeling of the reinforced concrete deep beam. This is another approach to the experimental examination which can often be rigorous and exorbitant. An eight-node solid element with one-point integration was employed for the beam mesh. An embedded truss reinforcement, the reinforcing bar was discretely modeled inside the FE mesh of the concrete elements to resemble the experimental study. The goal of the numerical analysis here is to determine the applicability of the concrete model of 3-dimensions simulation tools in producing the response of the deep beam similar to the experimental approach under the applied loading. The applicability of the software has been verified under the analysis of RCDBs with and without web openings (Quadri, 2023b). The reinforcing bars were discretized and arranged in the element mesh to allow it to behave as a beam structure. To mimic the experimental assessment, the setup geometry, boundary conditions, stress, and strength characteristics were replicated in the FEM. During the modeling process, the strength characteristics of each beam in **Table 1** were also taken into account. Each deep beam was modeled with the size of aggregate used in the experiment (50 mm, 25 mm, and 19 mm) as shown in **Fig. 3**. Unrealistic mesh sizes are avoided during modeling because mesh density is crucial in FEM since coarse meshing around complicated regions can yield incorrect findings. The support is modelled as simply supported and an applied concentrated load is exerted on the top. Both the supports and the loading point were modeled as elastic to avoid damaging the beam.

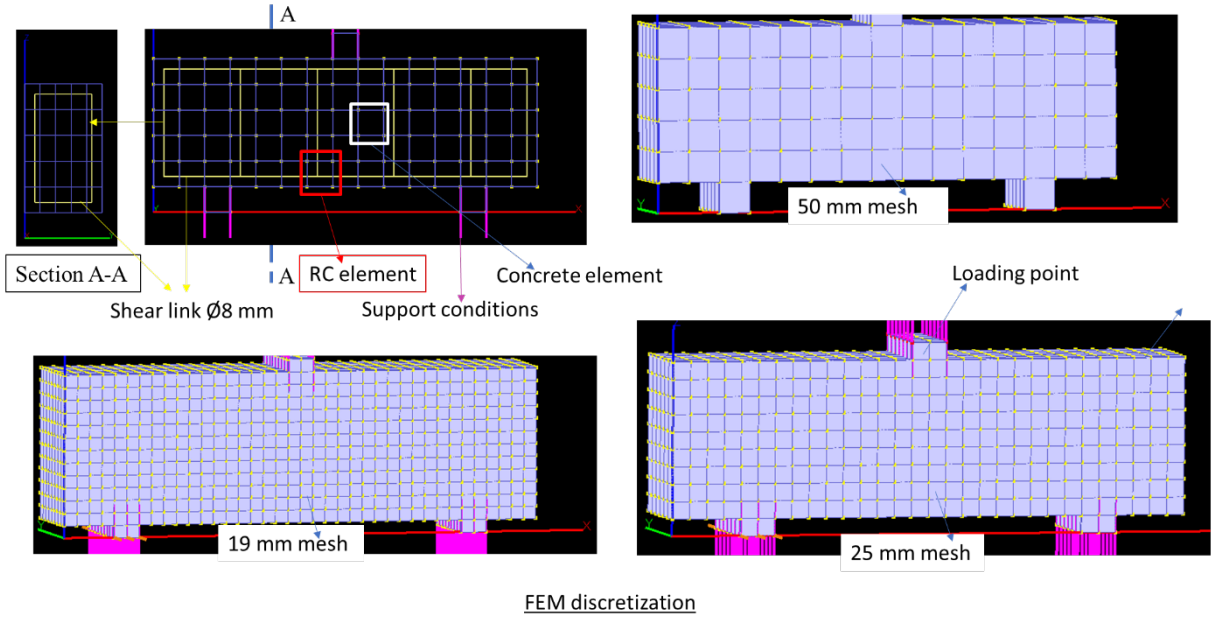

Fig. 3. FEM of the deep beam with different aggregate sizes

2.4 Global Response of RCDBs

The damage response of RCDB is attributed to a sharp diagonal crack that emerges within the shear distance which has no reckon on the flexural cracks. The cracks develop at the lower side of the beam adjacent to the support and travel diagonally to the compression zone, as shown in **Fig. 4**. The external load at the region of the point load may culminate the damage under compression failure if the speed of loading is high, the global failure may form a tied arch action enhancing the beam shear strength. This kind of response has been connected to the result from the stresses suffered by the tension bar which is transferred to crack concrete through the bond effect at the ultimate state (Quadri et al., 2024).

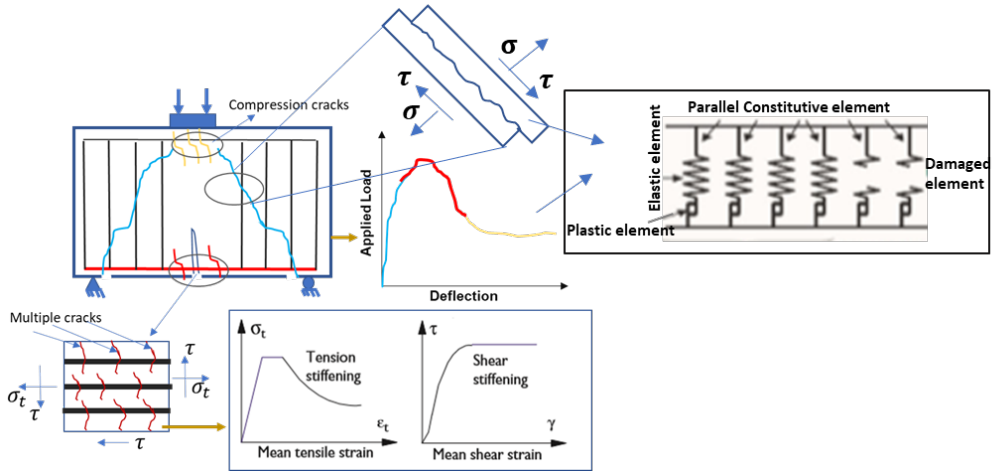

Fig. 4. Damage response of RCDB

3. Results and discussion

3.1 The failure mode of RCDB without web reinforcement

The damage response of beams without considering web reinforcement with different aggregate sizes under increasing monotonic load is presented in **Fig. 5**. In the case of the beam with a 50 mm aggregate beam (B1), the crack was initially observed at the flexural region at a capacity of 33 kN, which increased with an increase in the applied load. The angle of crack propagation changed suddenly at 55 kN in the middle of the beam and formed a split damage towards the compression zone resulting in brittle damage at the failure capacity of 79 kN. The measured crack width is 4 mm. In the case of a 25 mm aggregate beam (B2), the crack was also initiated at the flexural region at a capacity of 30 kN and propagated towards the middle of the beam at around 42 kN. An increase in load led to the initiation of a diagonal crack from the right-side support which propagated towards the compression zone while the previous crack increased in width at about 62 kN. This crack was bridged by the previous crack resulting in the initiation of another inclined crack that resulted in the damage at a capacity of 79 kN. The measured crack width is 2.1 mm. The failure response of the 19 mm aggregate beam (B3) is shearing damage which is initiated at 32 kN with a faint crack at the left-side support. An increase in the applied load resulted in several cracks forming around the big one. The final failure capacity is 80.6 kN, while the measured crack width is 1.1 mm.

The damage response of RCDB without web reinforcement appears to be affected by aggregate size, and the fracture propagation mode differs. The crack traveled through the weakest zone of the 50 mm aggregate beam, and the aggregate resisted the crack at a point where the angle orientation of travel changed. The 50 mm size aggregate in the concrete matrix allows a lot of voids filled by cement mortar which formed the weak zone, upon loading, propagation of cracks travelled through this zone leading to the tension damage. The tension reinforcement withstood the majority of the bar's load creating a dowel of the reinforcement. The 25 and 19 mm aggregate beams resisted the fracture, resulting in a lesser crack width than the 50 mm, which could be attributed to the aggregate pack volume. A similar damage mode has been reported by (Albidah et al., 2023b) using a 20 mm aggregate-size beam.

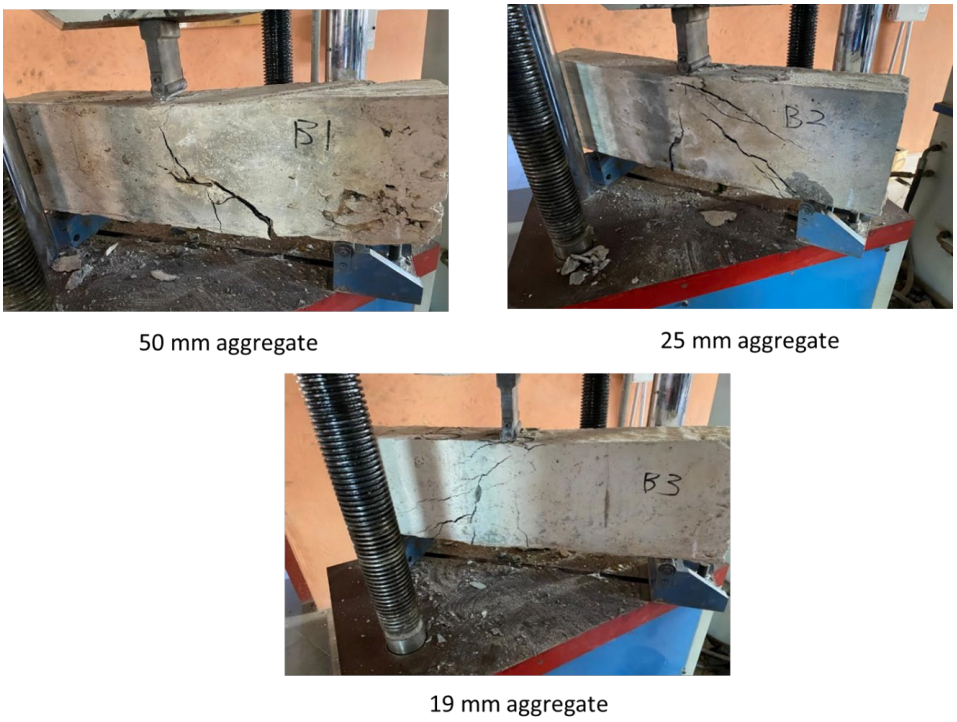

Fig. 5. Damage mode of beams with tensile reinforcement

3.2 Failure response of RCDBs with shear reinforcement

Figs. 6–8 show the response of RCDB with shear links for improving the shear capacity under the applied load. Beams with different aggregates presented here are duplicated with similar properties to observe the response under monotonic loading. **Fig. 6** is the damage response of beams with 50 mm aggregate (B1S1 and B1S2), **Fig. 7** depicts the damaged beam of 25 mm aggregate (B2S1 and B2S2), while **Fig. 8** shows the damaged beam of 19 mm aggregate (B3S1 and B3S2). Flexural cracks were initially observed in all beams which progressively developed into shear cracks except in B1S1 culminating in compression failure. The crack was initiated at the tension zone with a capacity of 48 kN for B1S1 and 55 kN for B1S2. A rise in the monotonic load caused compression damage to the beams while spalling of concrete was noted in B1S1, leading to rapid damage at a failure load of 86 kN, and diagonal cracking of B1S2 at a failure load of 98 kN. The crack propagation in

the beams behaves irrationally traveling through the weak zone of the concrete matrix, this could be due to considerable space between aggregates filled by mortar. The shear reinforcement resisted the majority of the stress generated enhancing the capacity of the beam. The initial crack load of beams B2S1 and B2S2 in **Fig. 7** is approximately 45 kN, and the flexural cracks spread progressively toward the compression zone. At roughly 73 kN, a shear fracture was developed at the left support of B2S1 and propagated to meet the flexural crack at the compression zone, resulting in compression damage to the beam with a capacity of 103 kN. In the case of B2S2, the flexural cracking moved towards the compression zone at around 79 kN, and when the load rose, excess concrete spalling at the compression zone caused total beam damage around 105 kN. The damage scenario of B3S1 is similar to that of B2S1 but with a smaller crack width. The initial crack load of B3S1 was around 36 kN, which traveled to the middle of the beam before multiple shear cracks with failure capacities of 100 kN formed. The first observable crack in B3S2 formed at the left side support at 40 kN and spread to form shear cracks at around 54 kN. Failure capacity was 91 kN.

Fig. 6. Damage mode of 50 mm aggregate beam

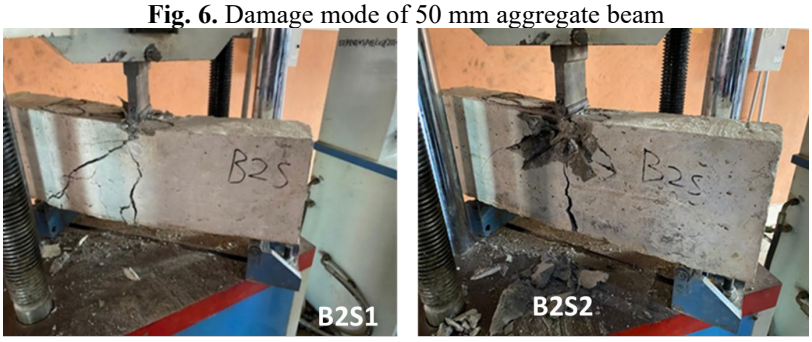

Fig. 7. Damage mode of 25 mm aggregate beam

Fig. 8. Damage mode of 19 mm aggregate beam

3.3 Load displacement curve response

The applied load versus displacement relationship of beams without web reinforcement having different sizes of aggregates is presented in **Fig. 9**. B1, B2, and B3 contain aggregate sizes of 50, 25, and 19 mm, respectively. The stiffness of the beams reduces gradually as the applied load increases. B3 has the highest stiffness with the highest initial crack and failure load of magnitude 32 and 80.6 kN, respectively with final displacement at failure load similar to the other beams. The stiffness here is when the load reaches the capacity of 75% (Vu et al., 2014). B1 stiffness diminishes after the emergence of a crack and deviates from linearity at around 57% (45 kN) of failure capacity at the displacement of 6 mm, after which nonlinearity emerges. In this case, the beams' behavior is characterized by unstable diagonal crack propagation; as shear cracks propagate, the fracture plane reaches a softening region, resulting in energy release and crack front advancement. B2 nonlinearity appears at 66% (52 kN) of its capacity when the shear crack begins from the support at the displacement of 7 mm, the shear crack propagation reaching around 78% of the total capacity. B3 shifts from linearity at around 73% (58 kN) of its failure capacity when the shear crack starts propagating at the displacement of 7 mm. The displacement at the failure load is 16.4 mm.

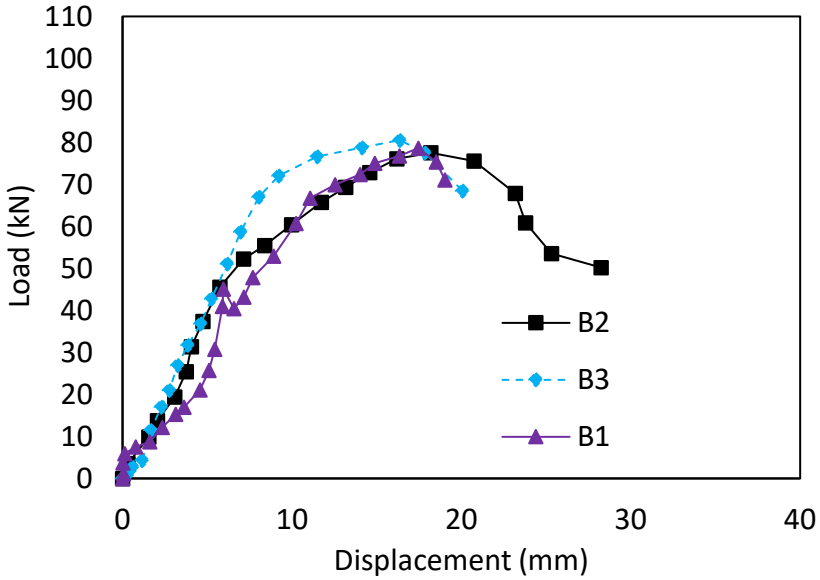

Fig. 9. Load vs displacement response of RCDB with longitudinal reinforcement

Fig. 10 shows the load against displacement comparison of experimental RCDBs with shear reinforcement of various aggregates. In general, the beams display initial elastic behavior in the pre-peak stress region, deviating from linearity as concrete cracks form. The reinforcement prevents fracture propagation, increasing the capacity of the beams. In the case of a 50 mm aggregate beam, B1S2 has 7% and 14% higher initial cracking and failure loads than B1S1, respectively, with no significant difference in displacement at failure load. The aggregate performed remarkably in the pre-peak region, resisting fracture development in the elastic zone. The 25 mm aggregate beams performed the best under the increasing monotonic loading with B2S2 having the highest initial cracking and failure loads among all the beams with different aggregates. B2S2 has a 4% failure load higher than B2S1 with no discrepancy in displacement value at failure load. The 19 mm aggregate size beams have the lowest initial crack value among the aggregate beams, B3S2 has a 10% higher initial cracking load than B3S1 but a 9% lower failure capacity. The web reinforcement provides an average of 27% increase in shear capacity over a beam without shear reinforcement, suggesting that the reinforcing bars absorbed significant loads when the concrete's tensile strength was surpassed and resisted concrete cracks. The post-peak zone is characterized by shear shear-stiffening response of reinforcement.

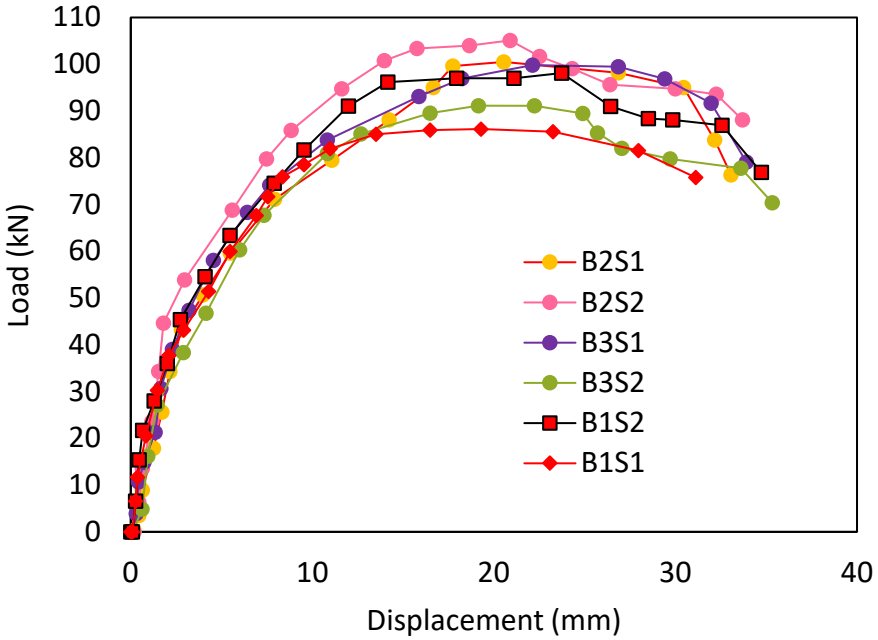

Fig. 10. Load vs displacement comparison response of RCDBs having different aggregates and shear reinforcement

3.4 Failure response of finite element model

The damage response of deep beams without web reinforcement simulated with different aggregate sizes under a finite element approach is presented in **Fig. 11** by the principal strain distribution. Generally, there is a high level of agreement

between the damage mode of numerical analysis and the experiment. The dominant damage under increasing loading is the diagonal shear cracks which emerged from the support section and traveled towards the underside of the loading point as soon as the tensile stress surpasses the tensile strength of the beam. The damage to the 50 mm aggregate is localized on the right side support; the initial crack appeared at 25 kN and proceeded diagonally to the loading point with crack width extension. The fracture propagation is comparable to the experiment, albeit with an 18% lower failure load. Flexural damage together with brittle shear cracks caused the collapse of 25 mm and 19 mm aggregate beams. In the case of a 25 mm aggregate beam, a flexural crack was initially observed at the concrete element (see **Fig. 3** for concrete element) at 22 kN, and an increase in the applied load resulted in the emergence of several flexural cracks that matured to form shear cracks and traveled toward the underside of the loading point at 76 kN. Crack initiation similar to what is observed on 25 mm aggregate also appeared on the 19 mm aggregate beam with nearly the same magnitude, the flexural cracks are more localized at the tensile zone. The damage occurred at 85 kN. Similar damage mode has been reported (Oviedo et al., 2016; Souza and Breña, 2016).

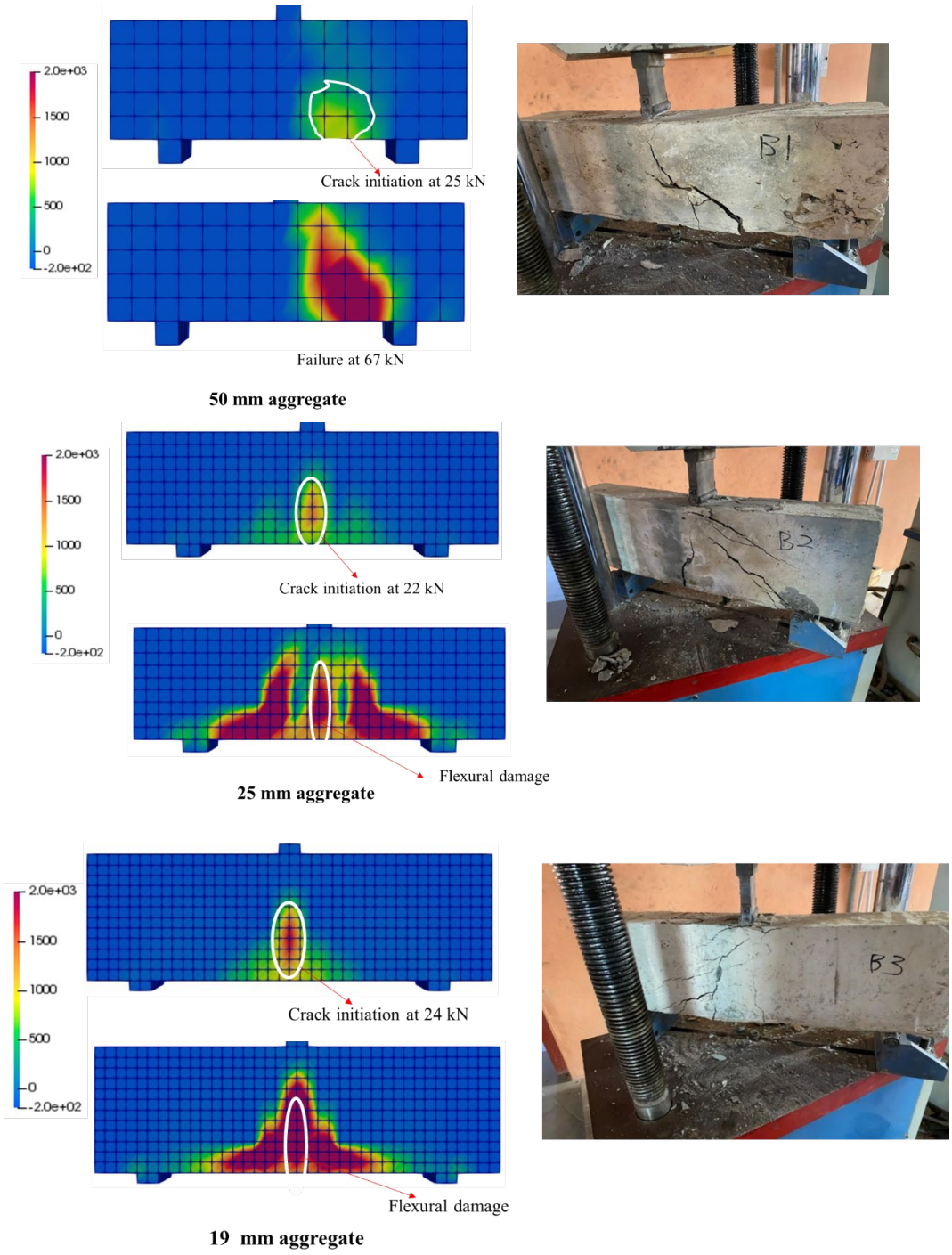

Fig. 11. Comparison of damage response of experiment and analysis of longitudinally reinforced beam of different aggregate size

The response of deep beams with different aggregates having shear reinforcement has been examined under the finite element model, the damage mode through the principal strain distribution is illustrated in **Fig. 12** to **Fig. 14**. The damage mode of the FEM 50 mm aggregate beam is compared with the experiment as shown in **Fig. 12**, the damage response acceded with the experiment, the crack emerged at the right side support at a capacity of 53 kN and traveled toward the middle portion of the beam at around 66 kN, a further increase in the load resulted in initiation of another crack at the left side support. The beam underwent compression damage at approximately 99 kN. The FEM damage response of a 25 mm aggregate beam under major strain distribution is shown in **Fig. 13**. At roughly 50 kN, a first crack appeared close to the flexural zone; when the monotonic load is increased, multiple flexural cracks could be seen on the left region. The cracks progressed to generate diagonal cracks at 83 kN capacity. The fracture has reached the compression zone at 105 kN, causing total beam collapse. The damage response of the experiment is successfully simulated under the FEM, the failure capacity is also assented with the experiment. In the case of the 19 mm aggregate beam, the crack occurred at the flexural zone similar to the experiment and travelled to the middle portion of the beam at around 55 kN, when the load was increased, a diagonal crack occurred at the right side and traveled towards the loading point, the damage occurred at 97 kN. The same damage mode has been observed by (Roy & Brena, 2008).

Although mesh optimization was considered for refined meshing of the FEM, the situation of real-life experiment may not be totally captured due to different sizes of mesh considered for experimental resemblance. Adequate design of reinforcement to resist brittle damage with other conservative design approaches may be necessary (Farouk et al., 2023b; Zhang et al., 2024). This will not only ensure compatibility and stability of the composite element but also ensures the nonlinear behaviour between steel and concrete is adequately evaluated.

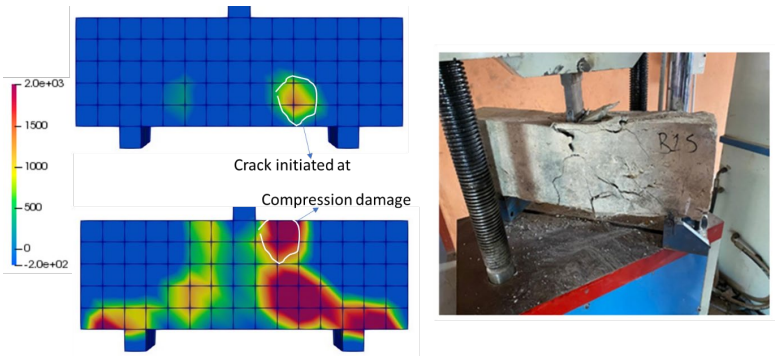

Fig. 12. Comparison of damage response of experiment and analysis of 50 mm aggregate beam with shear reinforcement

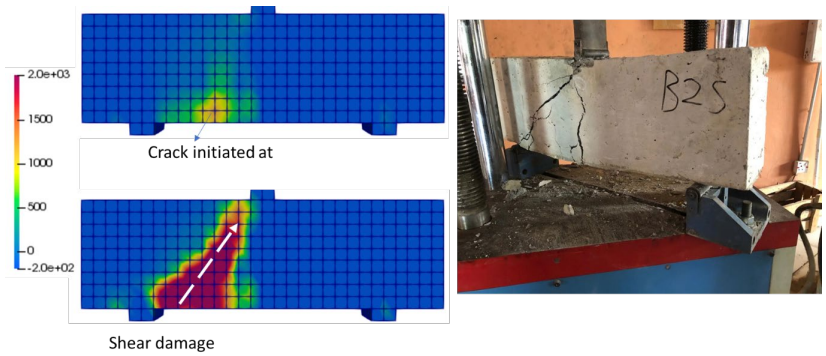

Fig. 13. Comparison of damage response of experiment and analysis of 25 mm aggregate beam with shear reinforcement

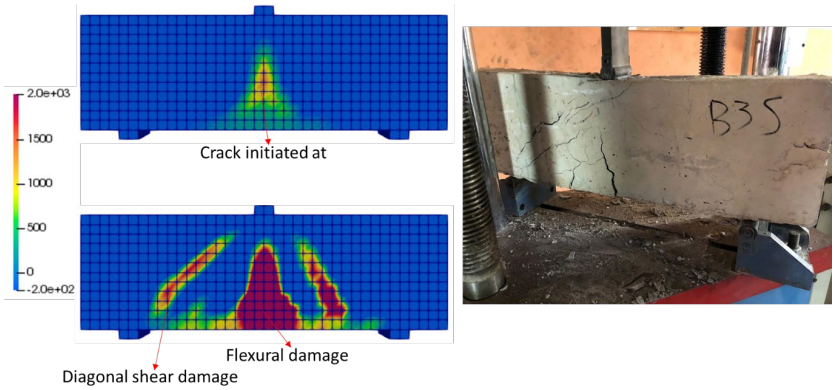

Fig. 14. Comparison of damage response of experiment and analysis of 19 mm aggregate beam with shear reinforcement

3.5 Load versus displacement comparison of the damage response between RCDBs test and FEM

Fig. 15 illustrates the comparison of the load versus displacement response of RCDBs without shear reinforcement between the FEM and experiment. The FEM displacement is derived from the loading point nodes. There is a distinct variation in the trend of displacement before failure, which is frequently influenced by the regularity of the mesh aggregate in the FEM. A close examination indicates that the stiffness in the FEM is higher than that of the experimental beam. Except for the 19 mm aggregate beam (B3), where the FEM has a higher failure capacity of 6% over the experiment, the experiment indicates no significant difference in capacity and displacement when compared to the FEM. Post-peak damage is characterized by nonlinear brittle damage caused by no reinforcement contribution other than aggregate interlock and concrete compressive strength. The comparison of the load versus displacement relationship between FEM and the experiment of RCDBs with shear reinforcement is presented in **Fig. 16**. A good conformity in the elastic linearity of the beams with almost similar stiffness can be seen. In **Fig. 16a**, deviation from linearity occurs among the beam at about 46 kN equivalent to displacement of 2.8 mm, which indicates the occurrence of concrete micro cracks. In **Fig. 16b**, the FEM beam deviates from linearity by 50 kN at 2.2 mm displacement, whereas the experiment averages 45 kN at 2.1 mm displacement. Deviation from elastic linearity occurs in FEM and experiments of 19 mm aggregate beams with displacements of 1.9 mm and 2.9 mm, respectively in **Fig. 16c**, with a similar load of 39 kN. In general, the load versus displacement response of the numerical analysis and the experiment are nearly identical, and beyond the elastic region, the reinforcement resisted the majority of the shear stress, particularly at the disturbed region of the beam, resulting in shear stiffening at the post crack region.

Table 2. Comparison of load and displacement of test beams

S/N	Beam type	Description	Crack load (kN)	Failure load (kN)	Displacement at initial crack (mm)	Displacement at final crack (mm)
1	**Beam with Tensile reinforcement**	**B1**	33	79	6	17.5
		FEM-B1	25	65	3	20
2		**B2**	30	79	4.6	18.5
		FEM-B2	22	76	2.8	17.8
3		**B3**	32	80.6	3.9	16.4
		FEM-B3	31	85	1.5	11.6
4	**Beam with Shear reinforcement**	**B1S1**	48	86	2.7	23.2
		B1S2	55	98	4.1	23.7
		FEM	53	99	4.6	28.9
5		**B2S1**	45	103	2.5	23.7
		B2S2	45	105	1.8	20.9
		FEM	50	105	2.2	23.3
6		**B3S1**	36	100	2.1	22.1
		B3S2	40	91	2.9	22.2
		FEM	55	97	3.3	33.8

Table 2 compares the load and displacement at the cracking and ultimate failure points. By using shear reinforcement, the 50 mm aggregate beam's shear capacity and ductility improved by 24% and 35%, respectively, compared to the beam without shear reinforcement. The 25 mm aggregate increased by 33% and 28%, while the 19 mm aggregate improved by 24% and 35%, respectively. The shear reinforcement increased the stiffness of the beam as well. Since aggregate resists the load by aggregate interlock action, it is crucial to choose the right aggregate when building concrete structural components. The results of this study will help engineers choose the best aggregate for a certain structural element.

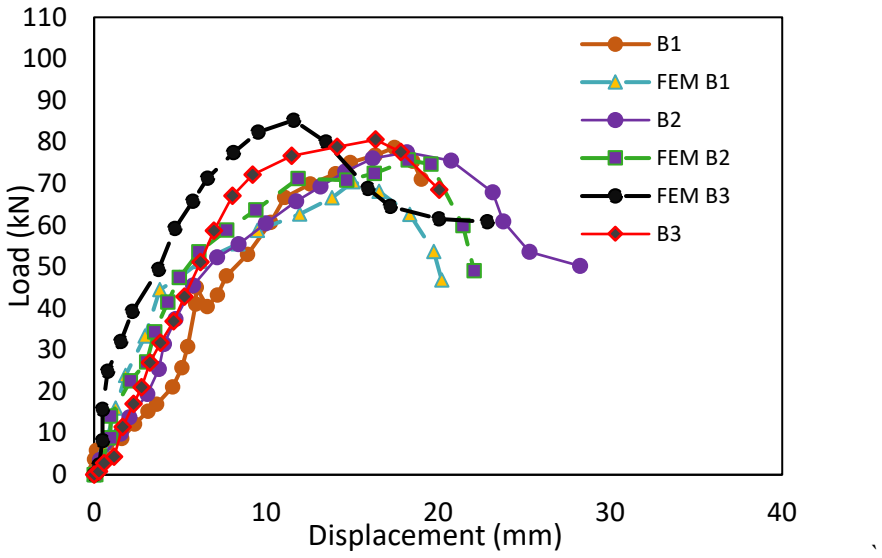

Fig. 15. Comparison of load versus displacement of the beam without shear reinforcement

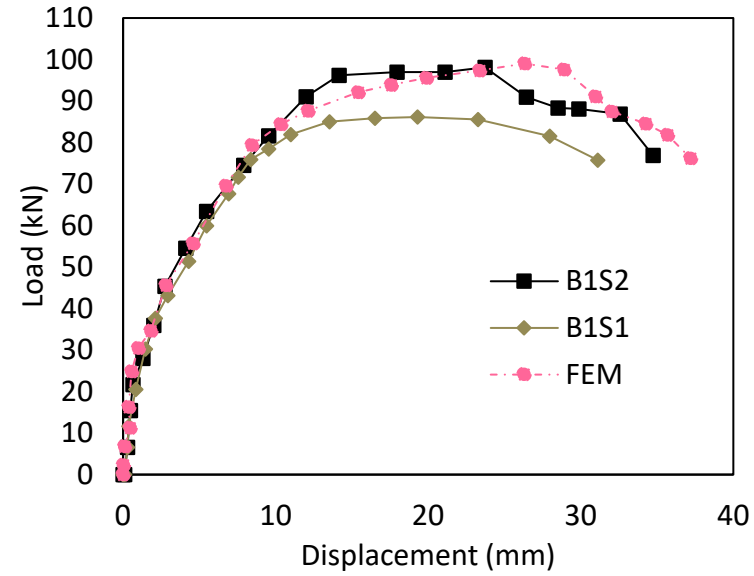

(a)

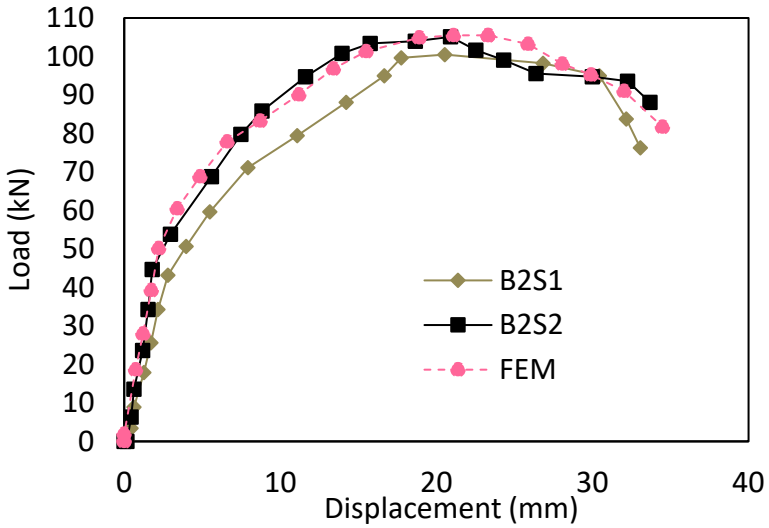

(b)

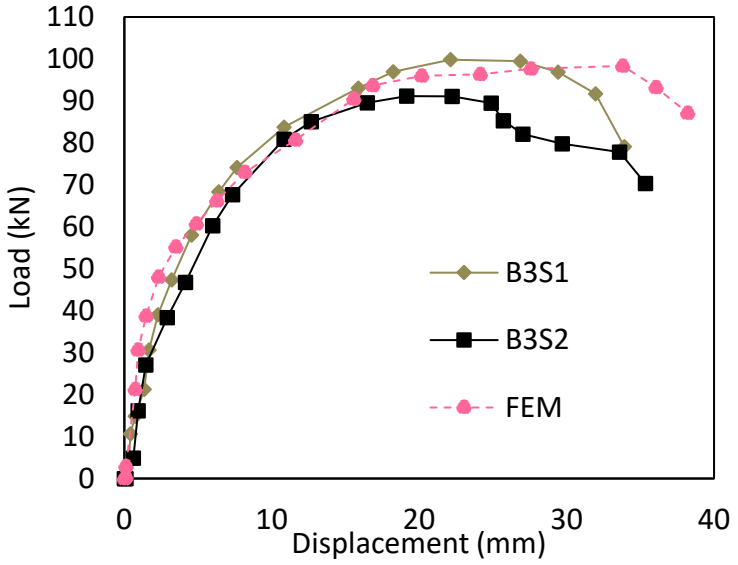

(c)

Fig. 16. Comparison of load versus displacement between FEM and experiment of RCDBs with shear reinforcement

3.6 Deep beam shear capacity prediction

There are numerous research on the response of RCDBs, some of which are purely analytical and adopt a finite element model, however, the shear design of RCDBs has not been fully understood. The shear at which the diagonal crack propagates at the disturbed region of reinforced concrete beams can be expressed as;

$$v_n = v_c + v_s + v_h \tag{1}$$

v_c is the shear contribution of concrete depending on the concrete compressive strength and the aggregate sizes. v_s is the shear contribution from vertical reinforcement while v_h horizontal reinforcement.
The empirically estimated shear strength of beams with and without shear reinforcement based on the ACI 318:05 shear equation has been modified to improve concrete shear prediction. The coarse aggregate effect, the unit weight of concrete, and the coarse aggregate impact characteristics were integrated into the model. As a result, the proposed equation is expressed as;

$$V_c = 0.8\sqrt{f'_{cu}}\left(\frac{W}{\rho}\left(\chi + \frac{\kappa\varphi}{a}\right)\right)bd \tag{2}$$

$$\chi = \left[0.74\left(\frac{f'_c}{105}\right)^3 - 1.28\left(\frac{f'_c}{105}\right)^2 + \left(\frac{f'_c}{105}\right) + 0.87\right] \tag{3}$$

where;

f'_{cu} is the compressive strength of concrete (N/mm^2), W is the unit weight of concrete (kg/m^3), ρ is the density of coarse aggregate (kg/m^3), χ is the correction factor for coarse aggregate as expressed in Eq. (3). κ is the aggregate crush value given in **Table 1**, φ is the coarse aggregate size in (mm), a is the shear span (mm), b is the width of the concrete section (mm), d is the the effective depth of the section (mm). The shear contribution from horizontal reinforcement can be expressed as given in Eq. (4).

$$v_h = A_h f_{yh}\left(2.5 - \frac{a}{d}\right) \tag{4}$$

The shear contribution from the vertical reinforcement (stirrups) can be expressed as given in Eq. (5).

$$v_s = A_s f_y\left(1 - \frac{1d}{2a}\right) \tag{5}$$

where A_h is the area of the longitudinal reinforcement, while A_s is the area of the vertical stirrups in (mm^2). f_{yh} is the yield strength of the longitudinal reinforcement, while f_y is the yield strength of stirrups measured in (N/mm^2). Thus, the shear strength of deep beams without web, v_n, (kN) reinforcement is estimated as given in Eq. (6), while the shear strength with web, v_{nw}, in (kN) reinforcement is expressed in Eq. (7).

$$v_n = 0.8\sqrt{f'_{cu}}\left(\frac{W}{\rho}\left(\chi + \frac{\kappa\varphi}{100a}\right)\right)bd + A_h f_{yh}\left(2.5 - \frac{a}{d}\right) \tag{6}$$

$$v_{nw} = 0.8\sqrt{f'_{cu}}\left(\frac{W}{\rho}\left(\chi + \frac{\kappa\varphi}{100a}\right)\right)bd + A_h f_{yh}\left(2.5 - \frac{a}{d}\right) + A_s f_y\left(1 - \frac{1d}{2a}\right) \tag{7}$$

The comparison of the test and predicted shear capacity of deep beams without web reinforcement is presented in **Fig. 17**. The shear capacity of the deep beam with web reinforcement is presented in **Fig. 18** which compares the tested beam to the predicted beam. There is no significant discrepancy between the estimated capacity of beams without web reinforcing and the test beams as shown by the error bar. In the case of 19 mm aggregate, the estimated capacity is 8 and 13% smaller than the experiment and FEM beam, respectively. In the case of a 25 mm aggregated beam, the predicted capacity is 3% less than the experiment and about 1% less than the FEM, but the predicted capacity in the case of a 50 mm aggregated beam is 2% less than the experiment and 11% higher than the FEM.

Furthermore, there is no significant discrepancy between the predicted shear capacity of RCDB with web reinforcement and the test beams. The predicted capacity is 3% lower than the test beam in the case of a 25 mm aggregate beam, while it is 3% higher than the test beam.

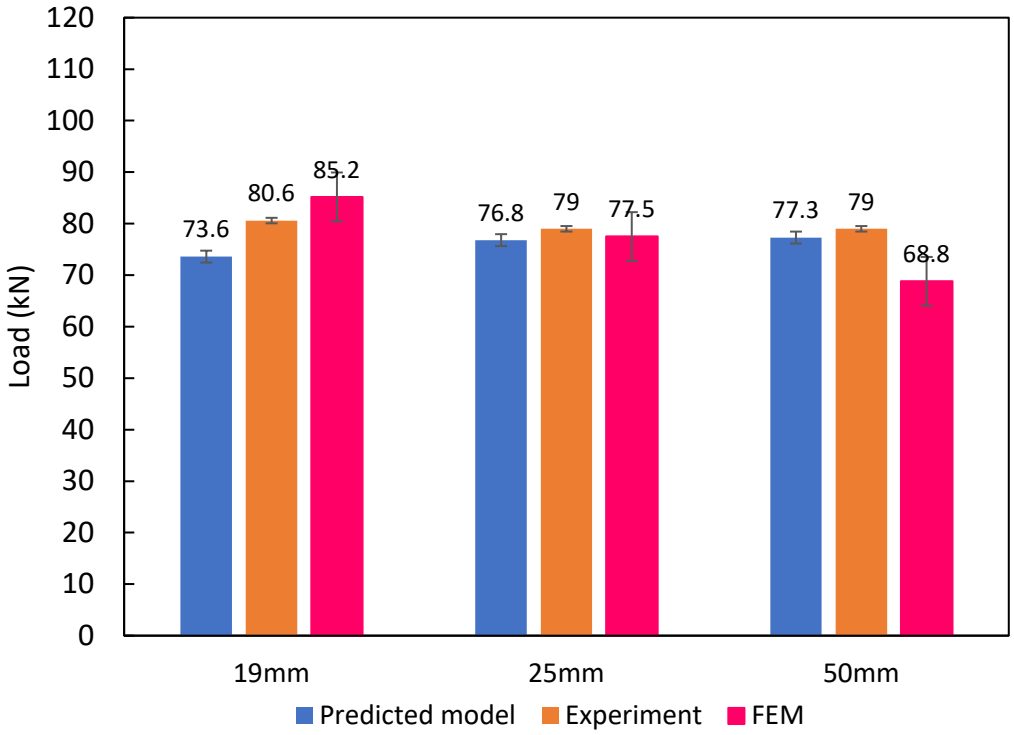

Fig. 17. Comparison of shear capacity of tested and predicted beam without web reinforcement

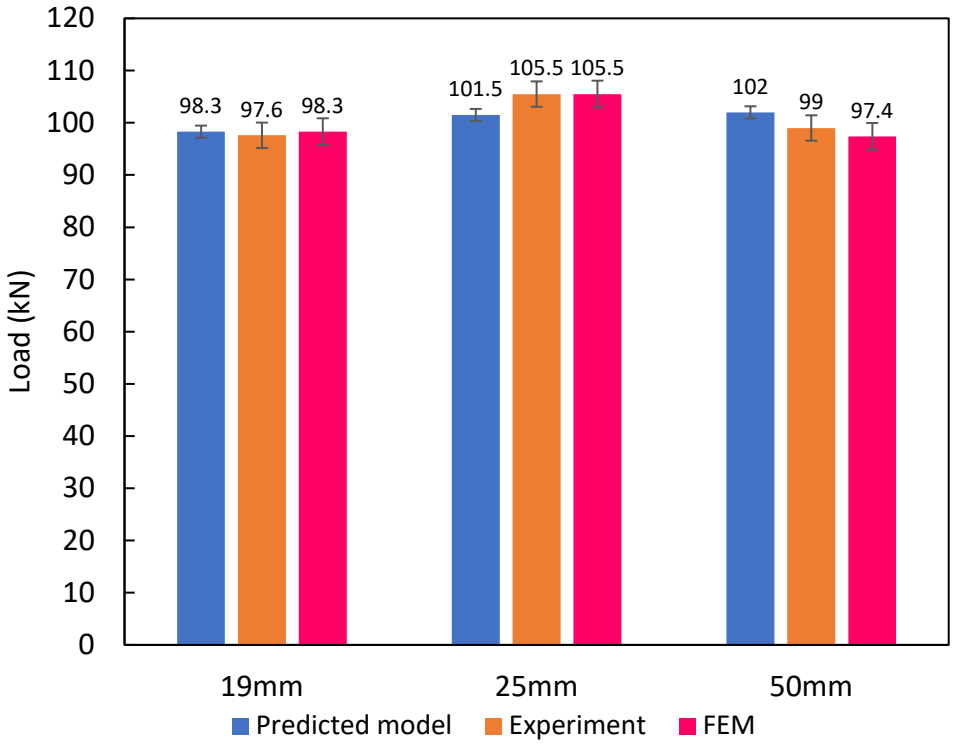

Fig. 18. Comparison of shear capacity of tested and predicted beam with web reinforcement

4. Conclusion

The response of RCDB containing different aggregate sizes has been examined experimentally and numerically under increasing monotonic loading. Nine beams were investigated with three without web reinforcement, while the rest contained web reinforcement. The following concluding remarks have been drawn.

1. The aggregate contributed to the damage mode of beams without web reinforcement; the 50 mm aggregate beam reduced multiple fracture propagations when compared to other aggregate-size beams. Furthermore, as demonstrated in the 25 mm aggregate size beam, strong compressive strength does not correlate to an increase in RCDB shear capacity.
2. The web reinforcement increases shear capacity by less than 30% on average over RCDB without shear reinforcement, implying that the reinforcing bars absorbed considerable loads when the tensile strength of the concrete was surpassed and

resisted the crack of concrete. The shear stiffness of reinforcement for all the aggregate size beams is similar at the pre-peak region, while shear stiffening occurred at the post-peak region.

3. The numerical analysis acceded well with the experiment in failure mode, in failure capacity, and in displacement. Beams without web reinforcement displayed a brittle damage mode while beams with web reinforcement exercised a shear stiffening behavior. The estimated model from the modified ACI 318:05 can predict the shear capacity of the RCDB with higher accuracy.

Data availability

The authors declare that the data supporting the findings of this study are available within the paper. Should any raw data files be needed, they are available from the corresponding author upon reasonable request.

Declaration of competing interest

The authors declare that they have no known competing financial interests or personal relationships that could have appeared to influence the work reported in this paper.

Funding

The authors received no financial support for the research authorship and/or publication of this article.

References

Abadel, A., Abbas, H., Almusallam, T., Alshaikh, I. M. H., Khawaji, M., Alghamdi, H., & Salah, A. A. (2022). Experimental study of shear behavior of CFRP strengthened ultra-high-performance fiber-reinforced concrete deep beams. *Case Studies in Construction Materials, 16*, e01103. https://doi.org/10.1016/j.cscm.2022.e01103

Abtan, Y. G., & Hassan, H. F. (2020). A Review Of Behavior of Reinforced Concrete Deep Beams. *Journal of Engineering and Sustainable Development, 24*(5), 66–77. https://doi.org/10.31272/jeasd.24.5.10

Accornero, F., Rubino, A., & Carpinteri, A. (2022). Post-cracking regimes in the flexural behaviour of fibre-reinforced concrete beams. *International Journal of Solids and Structures, 248*, 111637. https://doi.org/10.1016/j.ijsolstr.2022.111637.

ACI 318:05. (2005). Performance and Assessment Requirements for Design Standards on Structural Concrete (No. ISO 19338.2003(E)). aci. https://inspectapedia.com/structure/Building_code_requirements_for_structural_concrete-ACI.pdf

ACI Committee 318. (1999). Building code requirements for structural concrete: (ACI 318-99) And Commentry (ACI 318R-99). Farmington Hills, MI : American Concrete Institute, [1999] ©1999. https://ia800601.us.archive.org/6/items/1.ACI31899/1.%20ACI%20-318-99.pdf

Albidah, A. S., Alqarni, A. S., Wasim, M., & Abadel, A. A. (2023a). Influence of aggregate source and size on the shear behavior of high strength reinforced concrete deep beams. *Case Studies in Construction Materials, 19*, e02260. https://doi.org/10.1016/j.cscm.2023.e02260

Alius, F., Piscesa, B., Faimun, F., Alrasyid, H., & Iranata, D. (2020). Non-linear finite element analysis of reinforced concrete deep beam with web opening. *Journal of Civil Engineering, 35*(1), 3. https://doi.org/10.12962/j20861206.v35i1.7480

Alqarni, A. S., Albidah, A. S., & Abadel, A. A. (2022). Shear performance of reinforced concrete deep beams using different coarse aggregates under the effect of elevated temperatures. *Case Studies in Construction Materials, 16*, e01087. https://doi.org/10.1016/j.cscm.2022.e01087

Apebo, N. S., Iorwua, M. B., & Agunwamba, J. C. (2013). Comparative Analysis of the Compressive Strength of Concrete with Gravel and Crushed Over Burnt Bricks as Coarse Aggregates. *Nigerian Journal of Technology, 32*(1), 7–12.

ASTM C33/C33M-18. (2024). Specification for Concrete Aggregates. ASTM International. https://doi.org/10.1520/C0033_C0033M-18

Bamigboye, G., Ede, A., Umana, U., Odewumi, T., & Olowu, O. (2016). Assessment of Strength Characteristics of Concrete Made from Locally Sourced Gravel Aggregate from South-South Nigeria. *British Journal of Applied Science & Technology, 12*(5), 1–10. https://doi.org/10.9734/BJAST/2016/20365

Beshr, H., Almusallam, A. A., & Maslehuddin, M. (2003). Effect of coarse aggregate quality on the mechanical properties of high strength concrete. *Construction and Building Materials, 17*(2), 97–103. https://doi.org/10.1016/S0950-0618(02)00097-1

Bhattacharjee, E., Nag, D., Sarkar, P. P., & Haldar, L. (2011). An experimental investigation of properties of crushed over burnt brick aggregate concrete. *International Journal of Engineering Research and Technology, 4*(1), 21–30.

BS 8110. (1997). Code of Practice for Design and Construction of Reinforced Concrete. British Standards Institution.

BS 812-121. (1975). Testing aggregates. British Standards Institution.

BS EN 12390-5. (2009). Testing of Hardened Concrete. Flexural Strength of test Specimen. BSi.

Campione, G., & Minafò, G. (2012). Behaviour of concrete deep beams with openings and low shear span-to-depth ratio. *Engineering Structures, 41*, 294–306. https://doi.org/10.1016/j.engstruct.2012.03.055

Chen, C.-C., Lin, K.-T., & Chen, Y.-J. (2018). Behavior and shear strength of steel shape reinforced concrete deep beams. *Engineering Structures, 175*, 425–435. https://doi.org/10.1016/j.engstruct.2018.08.045

Chen, H., Wang, L., & Zhong, J. (2019). Study on an Optimal Strut-And-Tie Model for Concrete Deep Beams. *Applied Sciences, 9*(17), 3637. https://doi.org/10.3390/app9173637

Cho, S., & Kim, M. O. (2024). Effect of Aggregate Type on the Shear Behavior of Reinforced Lightweight Concrete Beams. *Applied Sciences, 14*(14), 5992. https://doi.org/10.3390/app14145992

Daneshfar, M., Hassani, A., Aliha, M. M., & Berto, F. (2022). Investigating Flexural Performance of Fiber-Reinforced Concrete with Different Contents and Types of Macrosynthetic Fiber. *Strength of Materials, 54*(4), 650-661. https://doi.org/10.1007/s11223-022-00443-x

Daneshfar, M., Hassani, A., Aliha, M. R. M., & Sadowski, T. (2023b). Assessment of the specimen size effect on the fracture energy of macro-synthetic-fiber-reinforced concrete. *Materials, 16*(2), 673. https://doi.org/10.3390/ma16020673.

Daneshfar, M., Hassani, A., Aliha, M. R. M., Sadowski, T., & Karimi, A. (2023a). Experimental Model for Study of Thickness Effect on Flexural Fatigue Life of Macro-Synthetic-Fiber-Reinforced Concretes. *Buildings, 13*(3), 642. https://doi.org/10.3390/buildings13030642.

El-Demerdash, W. E., El-Metwally, S. E., El-Zoughiby, M. E., & Ghaleb, A. A. (2016). Behavior of RC Shallow and Deep Beams with Openings Via the Strut-and-Tie Model Method and Nonlinear Finite Element. *Arabian Journal for Science and Engineering, 41*(2), 401–424. https://doi.org/10.1007/s13369-015-1678-x

Eurocode 2: Design of concrete structures. Part 1-1, General rules and rules for buildings. (2008). BSI.

Farouk, M. A., Moubarak, A. M. R., Ibrahim, A., & Elwardany, H. (2023). New alternative techniques for strengthening deep beams with circular and rectangular openings. *Case Studies in Construction Materials, 19*, e02288. https://doi.org/10.1016/j.cscm.2023.e02288

Gand, A., Mohammed, M., & Jarrouj, S. (2020). Performance of perforated FRP stub beams subject to static transverse actions. *Engineering Solid Mechanics, 8*(2), 105-118. 10.5267/j.esm.2019.10.004.

Gand, A., Sharif, S., Saidani, M., Lumor, R., Fom, P., Yeboah, D., & Ogbologugo, U. (2019). Performance of lightweight granulated glass concrete beams reinforced with basalt FRP bars. *Engineering Solid Mechanics, 7*(3), 247-262. doi: 10.5267/j.esm.2019.4.004

Golewski, G. L. (2023). The phenomenon of cracking in cement concretes and reinforced concrete structures: the mechanism of cracks formation, causes of their initiation, types and places of occurrence, and methods of detection—a review. *Buildings, 13*(3), 765. https://doi.org/10.3390/buildings13030765.

Hasan, K., Islam, M. T., Ferdaus, R., & Yahaya, F. M. (2023). Experimental study on environment-friendly concrete production incorporating palm oil clinker and cockle shell powder as cement partial replacement. *Materials Today: Proceedings*. https://doi.org/10.1016/j.matpr.2023.11.150

Hoseini, S. O., Mousavi, S. R., Sohrabi, M. R., & Ghasemi, M. (2023a). Using beam and ENDB specimens to evaluate fracture characteristics of wavy steel fiber-reinforced self-compacting concrete containing different coarse aggregate volumes. *Fatigue & Fracture of Engineering Materials & Structures, 46*(5), 1669-1686.https://doi.org/10.1111/ffe.13942.

Hoseini, S. O., Sohrabi, M. R., Mousavi, S. R., & Ghasemi, M. (2022). Effects of coarse aggregate and wavy steel fiber volumes on the critical stress intensity factors of modes I and III cracks in self-compacting concrete using ENDB specimens. *Theoretical and Applied Fracture Mechanics, 121*, 103421. https://doi.org/10.1016/j.tafmec.2022.103421.

Hoseini, S. O., Sohrabi, M. R., Mousavi, S. R., & Ghasemi, M. (2023b). Studying the rheological features, mechanical properties and flexural toughness of the WSFRSCC by varying the coarse aggregate volume. *Structures, 57,* 105115. https://doi.org/10.1016/j.istruc.2023.105115.

Hoseini, S. O., Sohrabi, M. R., Mousavi, S. R., Ghasemi, M., & Aliha, M. R. M. (2024). Comparing Different Procedures for Calculating Flexural Cracking Toughness Using Edge-Notched Disc Bend Specimen Under Modes I and III. *Fatigue & Fracture of Engineering Materials & Structures. 2024*, https://doi.org/10.1111/ffe.14530.

Ibrahim, M. A., El Thakeb, A., Mostfa, A. A., & Kottb, H. A. (2018). Proposed formula for design of deep beams with shear openings. *HBRC Journal, 14*(3), 450–465. https://doi.org/10.1016/j.hbrcj.2018.06.001

Institute of Civil Engineers. (1993). CEB-FIP Design Manual Application of the CEB-FIP Model Code 1978 for Concrete Structures. ICE Publishing. http://www.tocasa.es/zona2/CEB_FIP_model_code_1990_ing.pdf

Kim, K.-H., Kim, W.-B., Kim, J.-M., & Kim, S.-W. (2009). Composite Strut and Tie Model for Reinforced Concrete Deep Beams. *Journal of Advanced Concrete Technology, 7*(1), 97–109. https://doi.org/10.3151/jact.7.97

Kore, S. D., & Patil, S. S. (2013). Analysis and Design of R.C. Deep Beams Using Code Provisions of Different Countries and Their Comparison. *International Journal of Engineering and Advanced Technology, 2*(3), 166–170.

Liu, J., & Mihaylov, B. (2020). Shear strength of RC deep beams with web openings based on two-parameter kinematic theory. *Structural Concrete, 21*(1), 349–361. https://doi.org/10.1002/suco.201800356

Ma, C., Xie, C., Tuohuti, A., & Duan, Y. (2022). Analysis of influencing factors on shear behavior of the reinforced concrete deep beams. *Journal of Building Engineering, 45*, 103383. https://doi.org/10.1016/j.jobe.2021.103383

Megahed, K. (2024). Prediction and reliability analysis of shear strength of RC deep beams. *Scientific Reports, 14*(1), 14590. https://doi.org/10.1038/s41598-024-64386-w

Meyer, C. (2009). The greening of the concrete industry. *Cement and Concrete Composites, 31*(8), 601–605. https://doi.org/10.1016/j.cemconcomp.2008.12.010

Mohamed, A. R., Shoukry, M. S., & Saeed, J. M. (2014). Prediction of the behavior of reinforced concrete deep beams with web openings using the finite element method. *Alexandria Engineering Journal, 53*(2), 329–339. https://doi.org/10.1016/j.aej.2014.03.001

Mousavi, S., Ghasemi, M., & Dehghani, M. (2024). Investigating the fracture toughness of the self compacting concrete using ENDB samples by changing the aggregate size and percent of steel fiber. *Engineering Solid Mechanics, 12*(1), 17-26. doi: 10.5267/j.esm.2023.7.006

Nehdi, M. L. (2014). Clay in cement-based materials: Critical overview of state-of-the-art. *Construction and Building Materials, 51*, 372–382. https://doi.org/10.1016/j.conbuildmat.2013.10.059

Oviedo, R., Gutiérrez, S., & Santa María, H. (2016). Experimental evaluation of optimized strut-and-tie models for a dapped beam. *Structural Concrete, 17*(3), 469–480. https://doi.org/10.1002/suco.201500037

Quadri, A. I. (2020). Strut and Tie Modelling of Reinforced Concrete Deep Beams Under Static and Fixed Pulsating Loading. *Al-Nahrain Journal for Engineering Sciences, 23*(3), 306–312. https://doi.org/10.29194/NJES.23030306

Quadri, A. I. (2021). Assessment of reinforced concrete dapped end beams subjected to cyclic loading under bond deterioration and retrofitting approach. 横浜国立大学. https://doi.org/10.18880/00014111

Quadri, A. I. (2023a). Investigation of reinforced concrete members with bond deterioration under tensile load. *Materiales de Construcción, 73*(351), e319. https://doi.org/10.3989/mc.2023.297522

Quadri, A. I. (2023b). Shear response of reinforced concrete deep beams with and without web opening. *Innovative Infrastructure Solutions, 8*(12), 316. https://doi.org/10.1007/s41062-023-01286-4

Quadri, A. I., & Fujiyama, C. (2021). Response of Reinforced Concrete Dapped-End Beams Exhibiting Bond Deterioration Subjected to Static and Cyclic Loading. *Journal of Advanced Concrete Technology, 19*(5), 536–554. https://doi.org/10.3151/jact.19.536

Quadri, A. I., & Fujiyama, C. (2023). Assessment of repaired reinforced concrete dapped-end beams exhibiting bond deterioration under static and cyclic loading. *Construction and Building Materials, 403*, 133070. https://doi.org/10.1016/j.conbuildmat.2023.133070

Quadri, A. I., Lateef Oyedeji, A., Kehinde Kupolati, W., Ackerman, C., Snyman, J., & Musyoka Ndambuki, J. (2024). Performance evaluation of reinforced concrete culvert under monotonic loading. *Ain Shams Engineering Journal, 15*(11), 103001. https://doi.org/10.1016/j.asej.2024.103001

Quadri, A. I., Olanitori, L. M., & Sadiq, A. (2023). Effect of non-biodegradable waste materials on the strength performance of concrete. *Research on Engineering Structures and Materials, 9*(3), 1–13. https://doi.org/10.17515/resm2023.751st0428

Reddy, S. R., Kumar, B. S. C., & Monica, A. (2019). Comparitive Study on Behaviour of Deep Beams. *International Journal of Recent Technology and Engineering, 7*(6), 210–214.

Roy, N. C., & Brena, S. F. (2008). Behavior of Deep Beams with Short Longitudinal Bar Anchorages. *ACI Structural Journal, 105*(4), 460–470. https://doi.org/10.14359/19860

Saleh, M., AlHamaydeh, M., & Zakaria, M. (2023). Finite element analysis of reinforced concrete deep beams with square web openings using damage plasticity model. *Engineering Structures, 278*, 115496. https://doi.org/10.1016/j.engstruct.2022.115496

Souza, R. A., & Breña, S. (2016). Behavior predictions of deep beams with short straight bar anchorages using strut-and-tie models and nonlinear analysis. *Revista IBRACON de Estruturas e Materiais, 9*(5), 710–721. https://doi.org/10.1590/S1983-41952016000500004

Structural use of concrete (2nd ed). (1997). BSI.

Vu, N. S., Li, B., & Beyer, K. (2014). Effective stiffness of reinforced concrete coupling beams. *Engineering Structures, 76*, 371–382. https://doi.org/10.1016/j.engstruct.2014.07.014

Xu, S., Li, Q., Wu, Y., Dong, L., Lyu, Y., Reinhardt, H. W., ... & Hu, S. (2021). RILEM Standard: testing methods for determination of the double-K criterion for crack propagation in concrete using wedge-splitting tests and three-point bending beam tests, recommendation of RILEM TC265-TDK. *Materials and Structures, 54*, 1-11. https://doi.org/10.1617/s11527-021-01786-8.

Yang, K.-H., Chung, H.-S., Lee, E.-T., & Eun, H.-C. (2003). Shear characteristics of high-strength concrete deep beams without shear reinforcements. *Engineering Structures, 25*(10), 1343–1352. https://doi.org/10.1016/S0141-0296(03)00110-X

Yang, X., Wu, T., Liu, X., & Liu, Y. (2025). Influence of web reinforcement on shear behavior and size effect of lightweight aggregate concrete deep beams: Experimental and theoretical studies. *Engineering Structures, 322*, 119119. https://doi.org/10.1016/j.engstruct.2024.119119

Zhang, H.-Z., Luo, P., & Yuan, X.-X. (2024). Reinforcement layout design for deep beams based on bi-objective topology optimization. *Automation in Construction, 158*, 105237. https://doi.org/10.1016/j.autcon.2023.105237.